nature nanotechnology

LETTERS

https://doi.org/10.1038/s41565-019-0443-9

Gate-based high fidelity spin readout in a CMOS device

Matias Urdampilleta[1]*, David J. Niegemann[1], Emmanuel Chanrion[1], Baptiste Jadot[1], Cameron Spence[1], Pierre-André Mortemousque[1], Christopher Bäuerle[1], Louis Hutin[2], Benoit Bertrand[2], Sylvain Barraud[2], Romain Maurand[3], Marc Sanquer[3], Xavier Jehl[3], Silvano De Franceschi[3], Maud Vinet[2] and Tristan Meunier[1]*

The engineering of a compact qubit unit cell that embeds all quantum functionalities is mandatory for large-scale integration. In addition, these functionalities should present the lowest error rate possible to successfully implement quantum error correction protocols[1]. Electron spins in silicon quantum dots are particularly promising because of their high control fidelity[2–5] and their potential compatibility with complementary metal-oxide-semiconductor industrial platforms[6,7]. However, an efficient and scalable spin readout scheme is still missing. Here we demonstrate a high fidelity and robust spin readout based on gate reflectometry in a complementary metal-oxide-semiconductor device that consists of a qubit dot and an ancillary dot coupled to an electron reservoir. This scalable method allows us to read out a spin in a single-shot manner with an average fidelity above 98% for a 0.5 ms integration time. To achieve such a fidelity, we combine radio-frequency gate reflectometry with a latched spin blockade mechanism that requires electron exchange between the ancillary dot and the reservoir. We show that the demonstrated high readout fidelity is fully preserved up to 0.5 K. This result holds particular relevance for the future cointegration of spin qubits and classical control electronics.

The potential scalability and the recently reached high single qubit manipulation fidelities above 99.9% (ref. [5]) make electron spin qubits a promising candidate to build a quantum processor. Among the different strategies to build such a processor, the so-called surface code proposal[8] seems to be the most popular quantum error correction code. The surface code tolerates experimentally achievable error rates (less than 1%) and requires only nearest neighbour interaction in a simple two-dimensional (2D) arrangement of qubits[1].

However, to find a scalable high fidelity single-shot spin readout scheme is still an open challenge. Indeed, even though spin readout has been implemented in small 2D arrays[9–12], the problem of scalability imposes severe constraints on the gate layout[2,7], the positioning of the electron reservoirs and the charge readout strategy. Modern complementary metal-oxide-semiconductor (CMOS) technology offers the possibility to overcome these constraints by fabricating multilayer devices (3D architectures) in which local reservoirs and detectors can be implemented[13–15].

The single-shot detection of electron spins in semiconductor quantum dots (QDs) is based on a spin-to-charge conversion. This is achieved mainly through an energy-selective readout[16] or Pauli spin blockade (PSB)[17,18]. Then, the charge detection is usually implemented through the use of a quantum point contact or a single-electron transistor capacitively coupled to the probed system. This detection scheme allows a good readout fidelity at the cost of a large footprint, and cointegration becomes cumbersome as they require from one to three additional gates and two reservoirs. It precludes these methods from being integrated in a dense 2D array of QDs.

In this study, the charge detector is made of an ancillary QD tunnel coupled to a single reservoir and connected to a radio-frequency (RF) gate reflectometry set-up. In this scheme, the ancilla has an extended role with respect to standard gate reflectometry techniques[19,20] as it participates in the spin-to-charge conversion through a PSB mechanism. For this purpose, we used the triple gate device shown in Fig. 1a. It is fabricated from a silicon-on-insulator substrate with the standard CMOS technology (details in Methods). The ancilla QD underneath gate 1 is tunnel-coupled to a single reservoir and capacitively coupled to gate 1 (G1). G1 is directly connected to a tank circuit to achieve RF reflectometry[21,22] (Fig. 1b,c) and probe the charge configuration of the device. We first characterized the charge stability of the device, which is operated in a double QD configuration. For this purpose, we applied a positive voltage on G1 and G2 to form electrostatic QDs below each gate and we applied a negative voltage on G3 to isolate QD2 from the electron reservoir (Fig. 1b). The RF signal was sent to G1 and the reflected signal analysed. The corresponding demodulated signal (Fig. 1d) represents the change of amplitude induced by a change of capacitance between G1 and the channel. As a consequence, the degeneracy line seen on Fig. 1d is the signature of electrons tunnelling between one level of the QD under G1 and the reservoir.

As the G2 voltage is swept, discontinuities in the dot 1 (QD1) charge degeneracy line were observed. These discontinuities arise from changes in the charge occupation of QD2. QD1 appears to be a natural electrometer for QD2[23]. Below $V_{G2} = 0.5$ V, the discontinuities disappeared. We concluded that QD2 can be emptied at a lower voltage on G2 and that the few-electron regime was achieved in our CMOS device. From temperature-dependent spectroscopy, a lever arm of 0.3 was obtained and was similar for both gates (on their respective dots). The charging energy in the few-electron regime was estimated to be ~8 meV (~3 meV in the many-electron regime). This is comparable to measurements reported previously in CMOS QD devices[24]. Below, we focus on the region depicted in Fig. 1e where the PSB is used to perform a spin readout. This region corresponds to the chemical potential where the charge occupancy

[1]Univ. Grenoble Alpes, CNRS, Grenoble INP, Institut Néel, Grenoble, France. [2]CEA, LETI, Minatec Campus, Grenoble, France. [3]Univ. Grenoble Alpes, CEA, INAC-Pheliqs, Grenoble, France. *e-mail: matias.urdampilleta@neel.cnrs.fr; tristan.meunier@neel.cnrs.fr

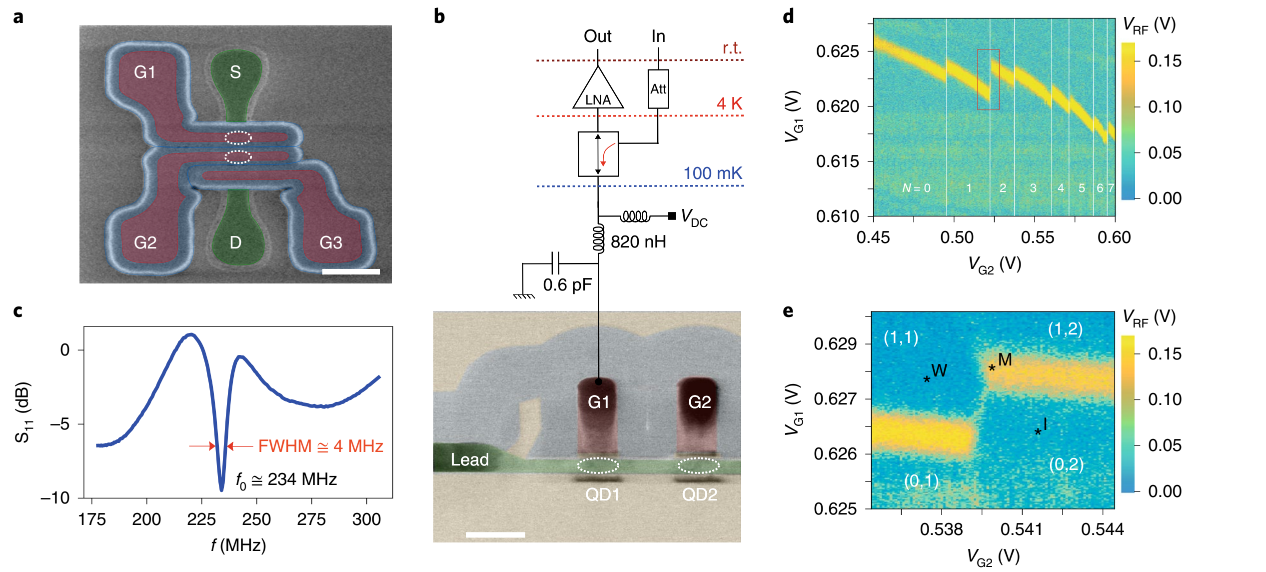

Fig. 1 | A CMOS device probed by gate-based RF reflectometry. a, Scanning electron micrograph of the CMOS device. The silicon wire (green) lies on the buried oxide layer and is covered with the three top gates (brown). Scale bar, 200 nm. **b**, The upper panel shows the reflectometry set-up, which comprises a tank circuit composed of an inductance and a parasitic capacitance to the ground. The injected signal, once reflected, is amplified using a cryogenic amplifier (LNA) and demodulated at room temperature (r.t.). The lower panel shows a transmission electron micrograph of a slice of a similar device. The two dots are located underneath G1 and G2. For simplicity, G3 is not represented as it is not used in this experiment. Scale bar, 40 nm. **c**, Reflected signal from the tank circuit. The resonator presents at low temperature a quality factor of ~50. **d**, The amplitude of the reflected signal is plotted as a function of G1 and G2 voltages. QD1 is strongly coupled to the reservoir and, as a consequence, a strong amplitude variation is visible for its charge degeneracy. When the total number of electrons in QD2 changes, it shifts the chemical potential of QD1, as highlighted by the solid white lines, where the number N stands for the number of electrons in QD2. **e**, The region framed by the red square in **d** shows the interdot transition from (0,2) to (1,1). The points I, W and M are used, respectively, to initialize, wait for relaxation and measure the spin. FWHM, full-width at half-maximum.

of QD2 changes from 1 to 2 and of QD1 from $N+1$ to N. As we observed the PSB at this transition we assumed that N is an even number—for simplicity, in the following we set $N=0$.

Spin-to-charge conversion was achieved by exploiting the PSB. To detect the PSB signature, we used a recently developed method[25–27], the so-called latched Pauli spin blockade (LPSB), which involves the conditional tunnelling of a third charge and therefore improves the amplitude of the spin-to-charge conversion as the total number of charges changes. This LPSB mechanism relies on the fact that the two QDs are not evenly coupled to the electron reservoir. In the present device, as to add a charge on QD2 is much slower than to add one on QD1. As a consequence, if we look at the triple point {(1,1), (0,2), (1,2)}, the charge transition (1,1) to (1,2) is much slower than (0,2) to (1,2). In terms of spin states, if the system forms a triplet state in (1,1), it would need first to relax to a singlet state before tunnelling to the (0,2) due to spin blockade, and then the transition to (1,2) can occur (Fig. 2a).

Figure 2b presents the single-shot signal obtained at the triple point M in the case of a singlet and a triplet state. In the case of a triplet state, the single-shot readout produces a step-like feature that is the signature of the finite lifetime of the LPSB. Therefore, we can discriminate between singlet and triplet states by looking at the detector initial value. The G1 voltage window where these events are observed is determined by the energy separation between singlet and triplet states in the (0,2) charge configuration, which is equal to the valley splitting in QD2 (Fig. 2a). We measured a valley splitting of 350 μeV (Supplementary Fig. 3) similar to that obtained in planar MOS devices[28].

To quantify the fidelity of the spin readout, we started by initializing the system in the singlet ground state by sitting in the (0,2) region for 50 ms. The system was then transferred to the (1,1) area where the singlet relaxes to the triplet ground state under a magnetic field. After 0.3 ms, there was an equal population in the singlet and triplet. The system was then pulsed to the point M to be measured. We analysed 10,000 of these sequences and the corresponding histogram is presented in Fig. 3a.

We obtained two distinct distributions that corresponded to the charge states (1,1) and (1,2), which give an average charge readout fidelity of 99.6%. This fidelity was limited by electrical noise, which induces a readout error at an average rate of 0.4%. However, when measuring the spin, the fidelity of the spin-to-charge conversion has to be quantified. In the present case, the LPSB had a finite lifetime (7 ms), which limits the integration time and degrades the spin readout fidelity. To estimate this fidelity at point M, we followed the method developed in Barthel et al.[18]: we fit the singlet probability distribution with a noise-broadened Gaussian distribution and the triplet one with a noise-broadened Gaussian distribution with an additional decay that accounts for the blockade lifetime at M (Supplementary Section 3 gives a detailed analysis). We defined the threshold between the singlet and triplet population as the point at which the visibility is maximum (Fig. 3b). We obtained a visibility higher than 97%, which gave singlet and triplet readout fidelities of 99.6% and 97.3%, respectively.

The error induced by the LPSB finite lifetime is the limiting factor of the readout fidelity at point M. However, as the system was displaced at different positions in the stability diagram prior to readout, errors during the preparation of well-defined states can also alter the global measurement. To quantify these errors, we used the protocol to start with a well-defined excited spin state that we let relax to the ground spin state and we then measured the transfer of population as a function of time. The initial and final population extracted experimentally allowed us to identify the different errors. To initialize a well-defined spin state, we first set the magnetic field to 3 T to separate the triplet ground state and the excited singlet

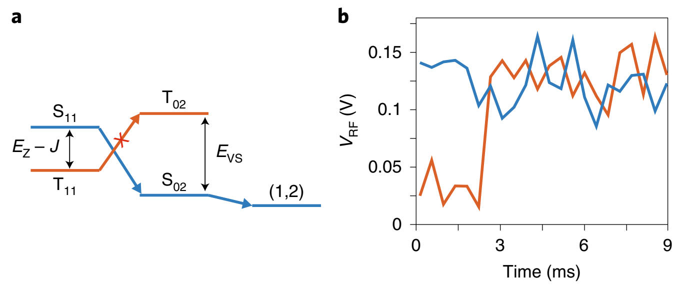

Fig. 2 | Single-shot spin readout. a, LPSB mechanism. In the (1,1) region, the triplet state T_{11} is the ground state when the Zeeman energy (E_Z) exceeds the exchange energy J. At the measurement point, where the exchange dominates, the singlet (blue) can tunnel from the (1,1) to the (0,2) state, which in turn can tunnel to the (1,2) state. However, the triplet state (orange) cannot tunnel to the (0,2) state due to the spin blockade and the (1,2) state cannot be reached. **b**, Single-shot measurement of the singlet and triplet states. The spin system is initialized in the singlet state and then moved to the W point (Fig. 1f), after some waiting time, the spin signal is measured by pulsing at point M. The blue (orange) curve shows a typical time trace at the measurement point, M, after a short (long) waiting time at W. The orange curve presents a low signal at the short measurement time as the system is stuck in the triplet (1,1) state. Once the triplet state has relaxed to the singlet state the spin blockade is lifted, which allows tunnelling, as shown by the signal at higher level. VS, valley splitting.

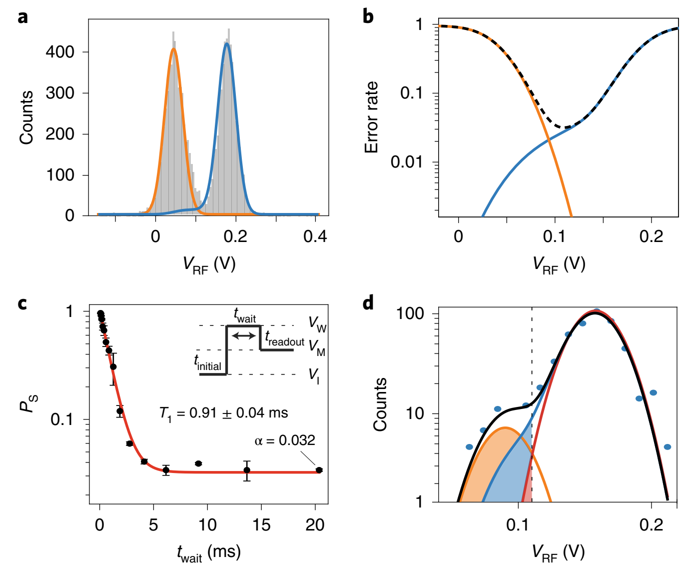

Fig. 3 | Spin readout error analysis. a, Histogram of 10,000 single-shot measurements integrated over a 500 µs integration time. The two distributions correspond to the two spin states, triplet (blue) and singlet (orange), and are fitted using a procedure described in the Supplementary Section 3 . **b**, The orange and blue solid lines correspond, respectively, to triplet and singlet readout error rate. The dashed line corresponds to $1-V$, where V is the visibility. At the point of maximum visibility, the error rate is below 3% for the triplet state and below 0.4% for the singlet state. **c**, P_S represents the probability to measure a singlet state at M at 3 T and is plotted as a function of the time spent at W (t_{wait}). The red solid line is an exponential fit. The residual value at a long t_{wait}, $\alpha=3.2\%$, accounts for all the different process that can lead to an error in spin labelling. The error on the population estimation is calculated from the fitting confidence of the two distributions. The inset shows the pulse sequence used to measure the relaxation curve. **d**, Histogram of single-shot measurements after preparing a triplet ground state ($t_{wait}=20$ ms). The red and orange solid lines are fits to a Gaussian model, the blue solid lines include a decay due to relaxation and the dashed black line indicates the spin-state threshold. The red area depicts the overlap error due to electrical noise in the measurement. The blue area depicts the error due to the finite LPSB lifetime. The orange area corresponds to a residual singlet due to the imperfect transfer between point W and M.

state with a Zeeman energy much larger than the thermal energy. We then prepared a singlet state by sitting for 50 ms at the point I in the (0,2) region (Fig. 1e). We pulsed the system at point W in the (1,1) region where we waited for a time t_{wait} to let the singlet state relax to the T_- ground state. Finally, the gates were pulsed to the measurement point M. Figure 3c presents such a measurement, with the singlet population at M plotted as a function of t_{wait}. From this plot, we extracted the relaxation time $T_1=0.91\pm0.04$ ms at point W. The plot also shows that the measured population of the singlet for a long t_{wait} is 3.2%, whereas the Boltzmann distribution at 3 T gives 10^{-7}%. Moreover, this cannot be explained by readout error, which has a rate smaller than 3%.

To analyse further this error, we plot in Fig. 3d the histogram of the triplet and singlet populations for $t_{wait}=20$ ms where the different error sources are represented by the coloured areas. The red area is the overlap between two Gaussian distributions and is the result of pure electrical noise. The blue area is the overlap between the singlet distribution (Gaussian) and the triplet distribution (Gaussian + single exponential decay), which is governed by the LPSB lifetime during the readout. Finally, the orange area corresponds to a finite singlet population that we estimated to be around 1.5%. We assumed that this singlet residue was created during the transfer of the triplet state from W to M. The same analysis was performed by preparing a triplet state that was then relaxed to the ground state in the (0,2) region. The corresponding plot and table containing the error analysis are presented in Supplementary Section 4 and Supplementary Fig. 4 .

To improve the spin readout fidelity, it is possible to tune two different parameters: the charge detection signal-over-noise ratio and LPSB lifetime. First, the signal can be improved by decreasing the tunnel coupling between the reservoir and the dot to increase the quantum capacitance and by reducing the parasitic capacitances. Second, our homemade cryogenic low-noise amplifier has a measured noise temperature of 70 K. This is more than two orders of magnitude larger than the noise temperature obtained with state-of-the-art superconducting amplifiers[29]. Using such amplifiers would allow a reduction of integration time below 10 µs with a similar signal over noise ratio. Finally, the LPSB lifetime, which is the limiting element in the present experiment, could be improved by tuning the interdot tunnel coupling[30]. By combining a short integration time with a long LPSB lifetime, we could envision a fidelity of 99.9% for 10 µs of readout time. Therefore, all the qubit operations (for example, one error correction cycle) could be performed in the few microsecond range, a time frame that makes large-scale computation viable in terms of computational run time.

Although the integration of a local reservoir makes the fabrication process more difficult, the present latching mechanism has some advantages compared with recent work on gate-based single-shot readout that relies on standard PSB[31,32]. First, it presents a longer blockade lifetime, which leads to a higher fidelity[27]. Second, the signal strength and the blockade lifetime could be tuned independently with two different tunnel couplings (reservoir to ancilla[21] and ancilla to qubit, respectively[30]). Better spin readout fidelities are then expected in comparison with the standard PSB, in which only the interdot tunnelling process controlled the two figures of merit. Finally, the tunnel coupling to a lead allows a fast spin initialization of the qubit and ancilla using, for instance, the spin-dependent tunnelling rate[12], which is not possible in a closed double QD.

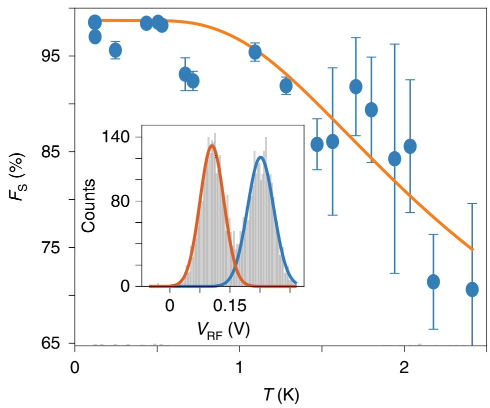

Fig. 4 | Temperature dependence of the singlet readout fidelity (F_S). The readout fidelity stays almost constant below 500 mK and drops drastically after 1 K. The model used to fit the data and extract the error bars accounts for thermal broadening of the detector's Coulomb peak (Supplementary Sections 3 and 5). The inset shows the two distributions at 1 K with a readout fidelity of 94%.

An interesting feature of the present readout procedure is the possibility to work at relatively high temperatures. Indeed, in contrast with the energy selective readout, the LPSB mechanism is based on spin-dependent tunnelling with no constraints on the ratio between the Zeeman and thermal energies. We investigated the temperature dependence of the readout fidelity up to 2 K at 3 T (Fig. 4). We can keep the readout fidelity above 95% up to 500 mK, which then decreases with temperature. Whereas the width of the distributions associated to each spin state are determined by the cryogenic amplifier noise (70 K) and are therefore insensitive to the temperature of the electrons, the separation between the maxima of the two distributions decreases with temperature due to the detector Coulomb peak broadening (Supplementary Fig. 5)[33]. The cross over, determined by the coupling between the detector and the reservoir, is estimated to be 150 μeV.

The measure of spin relaxation as a function of temperature (Supplementary Fig. 2) shows an increase of relaxation rate by only a factor of two between 0.1 K and 2 K. Being able to read out the spin of an electron at a higher temperature relaxes some constraints for the cointegration of a quantum processor together with classical control interface. Indeed, large-scale integration requires a complex control hardware whose thermal dissipation must be managed. Working at a higher temperature solves this issue as the cooling power evolves quadratically with temperature. Using modern cryogenics, we obtained more than 10 mW cooling power at 0.5 K. Therefore, we aim to develop a complex classical control system on the same chip as the quantum hardware and to use non-equilibrium manipulation schemes possible for spin qubits given their long relaxation time at 0.5 K, as shown by the present letter and recent experiments[34].

Here we demonstrate a high fidelity and robust spin readout using RF gate reflectometry in a CMOS double dot device. We show that the fidelity is limited by the ratio between integration time and the finite lifetime of the spin blockade, both of which can be improved experimentally. Our procedure, as well as those presented recently in a different QD architecture[31,32], is compatible with a scalable architecture in which helper dots connected to a single reservoir are locally coupled to each electron spin qubit of the 2D array[14]. To have local reservoirs could greatly simplify the electron loading and qubit initialization procedures of the 2D electron spin qubit array. Proposals to engineer a microsecond timescale and multiplexed high fidelity readout with an optimized RF set-up would put electron spin qubit in a favourable position to perform quantum information processing.

Online content

Any methods, additional references, Nature Research reporting summaries, source data, statements of code and data availability and associated accession codes are available at https://doi.org/10.1038/s41565-019-0443-9.

Received: 27 September 2018; Accepted: 29 March 2019;
Published online: 13 May 2019

References

1. Fowler, A. G. Two-dimensional color-code quantum computation. *Phys. Rev. A* **83**, 042310 (2011).
2. Veldhorst, M., Eenink, H. G. J., Yang, C. H. & Dzurak, A. S. Silicon CMOS architecture for a spin-based quantum computer. *Nat. Commun.* **8**, 1766 (2017).
3. Zajac, D. M. et al. Resonantly driven CNOT gate for electron spins. *Science* **359**, 439–442 (2018).
4. Watson, T. F. et al. A programmable two-qubit quantum processor in silicon. *Nature* **555**, 633–637 (2018).
5. Yoneda, J. et al. A quantum-dot spin qubit with coherence limited by charge noise and fidelity higher than 99.9. *Nat. Nanotechnol.* **13**, 102–106 (2018).
6. Maurand, R. et al. A CMOS silicon spin qubit. *Nat. Commun.* **7**, 13575 (2016).
7. Li, R. et al. A crossbar network for silicon quantum dot qubits. *Sci. Adv.* **4**, eaar3960 (2018).
8. Fowler, A. G., Mariantoni, M., Martinis, J. M. & Cleland, A. N. Surface codes: towards practical large-scale quantum computation. *Phys. Rev. A* **86**, 032324.
9. Thalineau, R. et al. A few-electron quadruple quantum dot in a closed loop. *Appl. Phys. Lett.* **101**, 103102 (2012).
10. Flentje, H. et al. A linear triple quantum dot system in isolated configuration. *Appl. Phys. Lett.* **110**, 233101 (2017).
11. Mukhopadhyay, U., Dehollain, J. P., Reichl, C., Wegscheider, W. & Vandersypen, L. M. K. A 2 × 2 quantum dot array with controllable inter-dot tunnel couplings. *Appl. Phys. Lett.* **112**, 183505 (2018).
12. Mortemousque, P. A. et al. Coherent control of individual electron spins in a two dimensional array of quantum dots. Preprint at https://arxiv.org/abs/1808.06180 (2018).
13. Batude, P. et al. 3D Sequential integration: application-driven technological achievements and guidelines. In *2017 IEEE International Electron Devices Meeting* 311 (IEEE, 2017).
14. Hutin, L., De Franceschi, S., Meunier, T. & Vinet, M. Quantum device with spin qubits. US provisional patent 15967778 (2018).
15. Larrieu, G. & Han, X.-L. Vertical nanowire array-based field effect transistors for ultimate scaling. *Nanoscale* **5**, 2437–2441 (2013).
16. Elzerman, J. M. et al. Single-shot read-out of an individual electron spin in a quantum dot. *Nature* **430**, 431–435 (2004).
17. Ono, K., Austing, D., Tokura, Y. & Tarucha, S. Current rectification by Pauli exclusion in a weakly coupled double quantum dot system. *Science* **297**, 1313–1317 (2002).
18. Barthel, C., Reilly, D. J., Marcus, C. M., Hanson, M. P. & Gossard, A. C. Rapid single-shot measurement of a singlet-triplet qubit. *Phys. Rev. Lett.* **103**, 160503 (2009).
19. Petersson, K. et al. Charge and spin state readout of a double quantum dot coupled to a resonator. *Nano Lett.* **10**, 2789–2793 (2010).
20. Colless, J. I. et al. Dispersive readout of a few-electron double quantum dot with fast RF gate sensors. *Phys. Rev. Lett.* **110**, 046805 (2013).
21. Gonzalez-Zalba, M. F., Barraud, S., Ferguson, A. J. & Betz, A. C. Probing the limits of gate-based charge sensing. *Nat. Commun.* **6**, 6084 (2015).
22. Urdampilleta, M. et al. Charge dynamics and spin blockade in a hybrid double quantum dot in silicon. *Phys. Rev. X* **5**, 031024 (2015).
23. House, M. G. et al. High-sensitivity charge detection with a single-lead quantum dot for scalable quantum computation. *Phys. Rev. Appl.* **6**, 044016 (2016).
24. Hofheinz, M. et al. Simple and controlled single electron transistor based on doping modulation in silicon nanowires. *Appl. Phys. Lett.* **89**, 143504 (2006).
25. Nakajima, T. et al. Robust single-shot spin measurement with 99.5% fidelity in a quantum dot array. *Phys. Rev. Lett.* **119**, 017701 (2017).
26. Fogarty, M. A. et al. Integrated silicon qubit platform with single-spin addressability, exchange control and single-shot singlet–triplet readout. *Nat. Commun.* **9**, 4370 (2018).
27. Harvey-Collard, P. et al. High-fidelity single-shot readout for a spin qubit via an enhanced latching mechanism. *Phys. Rev. X* **8**, 021046 (2018).
28. Yang, C. et al. Spin-valley lifetimes in a silicon quantum dot with tunable valley splitting. *Nat. Commun.* **4**, 2069 (2013).
29. Macklin, C. et al. A near-quantum-limited Josephson traveling-wave parametric amplifier. *Science* **350**, 307–310 (2015).

30. Maisi, V. F. et al. Spin-orbit coupling at the level of a single electron. *Phys. Rev. Lett.* **116**, 136803 (2016).
31. West, A. et al. Gate-based single-shot readout of spins in silicon. *Nat. Nanotechnol.* https://doi.org/10.1038/s41565-019-0400-7 (2019).
32. Pakkiam, P. et al. Single-shot single-gate rf spin readout in silicon. *Phys. Rev. X* **8**, 041032 (2018).
33. Beenakker, C. W. J. Theory of Coulomb-blockade oscillations in the conductance of a quantum dot. *Phys. Rev. B* **44**, 1646 (1991).
34. Petit, L. et al. Spin lifetime and charge noise in hot silicon quantum dot qubits. *Phys. Rev. Lett.* **121**, 076801 (2018).

Acknowledgements
We acknowledge technical support from P. Perrier, H. Rodenas, E. Eyraud, D. Lepoittevin, I. Pheng, T. Crozes, L. Del Rey, D. Dufeu, J. Jarreau, C. Hoarau and C. Guttin. The European Union's Horizon 2020 research and innovation programme supports M.U. through a Marie Sklodowska Curie fellowship (ODESI project). E.C. and C.S. acknowledge the Agence Nationale de la Recherche under the programme 'Investissements d'avenir' (ANR-15-IDEX-02). D.J.N. and C.S. acknowledge the GreQuE doctoral programmes (grant agreement no. 754303). The device fabrication is funded through the Mosquito project (grant agreement no. 688539). This work is supported by the Agence Nationale de la Recherche through the CMOSQSPIN and the CODAQ projects (ANR-17-CE24-0009 and ANR-16-ACHN-0029).

Author contributions
M.U. and T.M. conceived and designed the experiment. M.U., D.J.N., E.C. and T.M. performed the experiment and analysed the data. L.H., S.B. and M.V. designed the MOS devices and managed the fabrication process. M.U. and T.M. wrote the manuscript with input from all the authors.

Competing interests
The authors declare no competing interests.

Additional information
Supplementary information is available for this paper at https://doi.org/10.1038/s41565-019-0443-9.

Reprints and permissions information is available at www.nature.com/reprints.

Correspondence and requests for materials should be addressed to M.U. or T.M.

Journal peer review information: *Nature Nanotechnology* thanks Karl Petersson and other anonymous reviewer(s) for their contribution to the peer review of this work.

Methods

Materials and set-up. The device, depicted in Fig. 1a, was fabricated from a silicon-on-insulator substrate composed of a 145 nm buried oxide layer and an 11 nm thick silicon layer. The thin silicon film was patterned to create a 200 nm long and 30 nm wide nanowire by means of electron-beam lithography. Three 30 nm wide wrap-around top gates were defined using a SiO_2(2.5 nm)/HfO_2(1.9 nm) stack for the gate dielectric followed by TiN(5 nm)/poly-Si(50 nm) as the top gate material. The source and drain were self-aligned and formed by phosphorous ion implantation and annealing after the deposition of 20 nm long Si_3N_4 spacers. The device was anchored to the cold finger, which was in turn mechanically attached to the mixing chamber of a homemade dilution refrigerator with a base temperature of 80 mK. It was placed at the centre of a superconducting solenoid that generated the static out-of-plane magnetic field. The QDs were defined and controlled by the application of voltages on gates deposited on the surface of the crystal. Homemade electronics ensured fast changes of both chemical potentials and tunnel couplings with voltage pulse rise times approaching 100 ns and refreshed every 16 µs.

The tank circuit was composed of a surface-mounted inductance (820 nH), a parasitic capacitance to ground (0.6 pF) and the device capacitance between gate 1 and the device channel. The RF-gate reflectometry was performed close to the resonance frequency (234 MHz), with the input power set to −95 dBm and the reflected signal amplified by a low noise cryogenic amplifier anchored at the 4 K stage and by a room temperature low-noise amplifier. The signal was demodulated at room temperature, as shown in Fig. 1b, followed by 100 kHz filtering and amplification before digitalization. A switch was used to turn on the RF excitation only during the measurement sequence.

Data availability

The data that support the plots within this paper and other findings of this study are available from the corresponding author upon reasonable request.